



Effect of precursor chemistry on the structural and sensing properties of hydrothermally grown nanorods

Aniruddh Bahadur Yadav¹ · Padidepu V. L. Parvathi² · Shaik Ruba Thabassum²

Received: 21 February 2019 / Accepted: 28 May 2019 / Published online: 1 June 2019
© Springer-Verlag GmbH Germany, part of Springer Nature 2019

Abstract

We report on the effect of precursor chemistry on ZnO nanorods (NRs) growth and their hydrogen sensing characteristics probably for the first time. We found that zinc acetate grown nanorods were dislocated at the center and showed better sensitivity towards hydrogen gas than conventional NRs without dislocation. For nanorods growth, a ZnO seed layer of thickness 80 nm was deposited by RF sputtering at room temperature over SiO₂/p-Si substrate; oxidation in silicon substrate was done by the thermal oxidation method. The crystalline phases and the surface nanostructure of the ZnO thin film (seed layer) were investigated by the X-ray diffraction and atomic force microscope. The ZnO nanorods' surface morphology and their crystalline nature were studied by SEM and X-ray diffraction. The chemical properties of the ZnO nanorods were investigated by the X-ray photoluminescence spectroscopy. Using DC sputtering and shadow mask, Ti (80 nm)/Au (100 nm) metal layers were deposited over the ZnO nanorods to fabricate a metal semiconductor metal structure for sensor fabrication. *I*-*V* characteristics of the devices were obtained by the semiconductor parameter analyzer. The hydrogen gas was exposed over the devices using mass flow controller, and it was found that device containing nanorods grown by zinc acetate shows 98% sensitivity for 24 ppm gas concentration in a nitrogen atmosphere that was the largest reported till date than with bare conventional non-dislocated NRs.

1 Introduction

Hydrogen gas has emerged as an unconventional energy source for the fast developing twenty-first century to fulfill the rising demand for a pollution-free environment and energy need [1]. It is because hydrogen gas (H₂) is a highly combustible, nonpolluting and renewable energy source among the six alternatives to carbon-based energy sources and may be used efficiently in aircraft, automobiles, fuel cells, and chemical companies, etc. [2]. Some other important properties of this clean energy are it is nontoxic, light in weight, diffuses easily (with a coefficient of diffusion of 0.61 cm²/s in the air), abundant in nature, and highly inflammable (inflammability range is from 4 to

75%) [3]. Moreover, it is believed that even 4.65% hydrogen gas present in the air can cause a disastrous explosion [1]. Also, it is observed that a small amount of hydrogen gas (~0–2%) released in coal mines with methane gas can cause a severe blast. Also, because of its tiny molecular size and the leakage probability of hydrogen gas, its confinement and containment are very challenging for domestic as well as industrial applications. So, it is essential to develop a reliable hydrogen sensor to protect the humankind working with it or in an environment where it is released with other gases (e.g., coal mines). Considering this, a considerable amount of research has been focused on developing an efficient hydrogen sensor. Among the developed sensors till date, hydrogen sensors fabricated using catalytic metals and decorated one-dimensional metal oxide semiconductors like nanorods, nanoneedle, nanobelts as sensing platform have shown great potential.

In the metal oxide semiconductor family, ZnO has been attracting intensive attention for gas sensor fabrication in recent years because of its intrinsic properties like wide bandgap energy, robustness, room temperature lasing, resistance to radiation, optoelectronics, and being sensitive to many oxidizing and reducing gases [1–3]. Furthermore,

✉ Aniruddh Bahadur Yadav
ani84ani@gmail.com

¹ Department of Electronics and Communication Engineering, Velagapudi Ramakrishna Siddhartha Engineering College Kanuru, Vijayawada, Andhra Pradesh, India

² Nanoelectronics Lab, Department of Electronics Communication Engineering, Sree Vidyanikethan Engineering College, Tirupati, Andhra Pradesh, India

one-dimensional nanostructure particularly, ZnO nanorods have been synthesized and deposited by a range of physical and chemical methods and were utilized in sensor fabrication. Some of these deposition methods are chemical bath deposition [4], thermal evaporation [5], and hydrothermal method [6]. Among these various methods which have been generally utilized for deposition of ZnO nanorods, the hydrothermal method is advantageous because it is a relatively inexpensive, eco-friendly method, and the growth temperatures are very low ($\sim 90^\circ\text{C}$) [6–10]. Here we are presenting some of the important work that reported previously on hydrogen gas sensors fabricated on ZnO nanorods where NRs were synthesized by various methods. Tien et al. developed a Pt-coated ZnO nanorod-based hydrogen sensor [11]. Their sensor was able to detect 500 ppm of hydrogen concentration with 90% sensitivity [2]. Wang et al. fabricated a sensor using Pd cluster-decorated ZnO nanorods [12]. Their sensor showed 2.5–4.5% sensitivity for 10–500 ppm of hydrogen gas concentration. Ranawa et al. reported a Schottky diode-based hydrogen detector, which was fabricated by depositing silver on ZnO nanorods. This sensor successfully detected 1–5% hydrogen with 11–67% sensitivity [13]. Bhatia et al. fabricated a hydrogen sensor using nickel-doped ZnO nanorods, which shows 69% sensitivity for 1% of hydrogen concentration [14]. Kim et al. demonstrated amorphous palladium-decorated ZnO nanorod-based hydrogen sensor. The maximum sensitivity of this sensor was 27,000% for 6% of hydrogen in air. However, for 10 ppm hydrogen, the sensitivity of this specific sensor was only 20% [15]. Drawbacks associated with these sensors are complexity and high cost.

In the present work, two different precursor solutions, namely zinc acetate and zinc nitrate, were used in the hydrothermal reactors to grow ZnO nanorods on a single crystalline room temperature RF-deposited ZnO seed layers. Then using DC sputtering and shadow mask technique, Ti (80 nm)/Au (100 nm) metals layers were deposited over the nanorods to fabricate a metal semiconductor metal, a simple structured and low-cost sensor for hydrogen gas detection. As per the knowledge of the authors, till date, no report is available on nanostructure dislocation in nanorods depending on precursor chemistry. Nanostructure dislocation dependency on hydrogen gas-sensing properties of the nanorods has also not been studied.

2 Experiment

A p-type silicon substrate was used for the nanorods' growth and device fabrication for hydrogen sensing. To isolate the nanorods from the silicon substrate, a 200 nm oxide layer was grown by a dry oxidation method reported elsewhere [7]. On the oxide layer, 80-nm-thin ZnO seed layer was

deposited using RF sputtering. Before introducing argon gas into deposition chamber, the pressure was 1.5×10^{-6} mbar using vacuum pump. Processing pressure was fixed at 1.6×10^{-2} mbar with an argon gas flow rate of 15 sccm. Substrates were kept at 27°C and deposition was carried out at a constant radio frequency power of 100 W. On these ZnO thin films (acts as seed layer) using the hydrothermal method, nanorods array were grown. For nanorods deposition, an equimolar aqueous solution was obtained by mixing zinc nitrate (25 mM) and hexamethylenetetramine in a borosilicate beaker. Similarly, another equimolar aqueous solution was obtained by mixing zinc acetate (25 mM) and hexamethylenetetramine in another borosilicate glass beaker [16]. Then, ZnO thin film-coated substrates were placed in a homemade clamp to keep the seeded surface facing the beaker bottom, and this clamp was put in these two beakers containing two precursor solutions. After this, the beakers were sealed and put into a laboratory hot oven whose temperature was increased to 95°C and fixed for 4 h. The time of growth of the ZnO nanorods was 4 h. After growth, the samples were removed from the beaker and rinsed with deionized water many times, then water droplets on the coated substrate were dried by blowing N_2 at room temperature. From now on, the substrates containing the nanorods grown in zinc acetate and zinc nitrate precursor solution are called S1 and S2. Ti (80 nm)/Au (100 nm) metal layers were deposited onto the ZnO NRs, which were deposited in two precursor aqueous solutions as described previously, using DC sputtering and shadow mask technique. The schematic of the metal–semiconductor–metal chemiresistive hydrogen gas sensor is shown in Fig. 1a. Surface nanostructure of the ZnO seed layer was studied by atomic force microscope (AFM) (AFM-PICO SPM, Pico scan 210). The crystalline phase and nanostructure morphology of the ZnO nanorods were investigated by X-ray diffraction (XRD) using a single wavelength radiation $\text{Cu-K}\alpha = 1.5406 \text{ \AA}$ and scanning electron microscope (SEM)(EVO18 ZEISS, Oberkochen, Germany). The chemical properties of the ZnO nanorods grown by these two different precursors were investigated by XPS (ULVAC-PHI, model PHI5000 Versa Probe II). The fabricated sensors' electrical characterization was done in air and hydrogen ambient environment using semiconductor parameter analyzer Proxima 1500A.

3 Results and discussion

Figure 1b shows the two-dimensional AFM image of ZnO thin film deposited by RF sputtering at room temperature, which was used as a seed layer to grow nanorods. Fig. 1c shows the three-dimensional image of this seed layer. The image shows the uniform distribution and *c*-axis orientation of grains in the ZnO thin film. The roughness of the

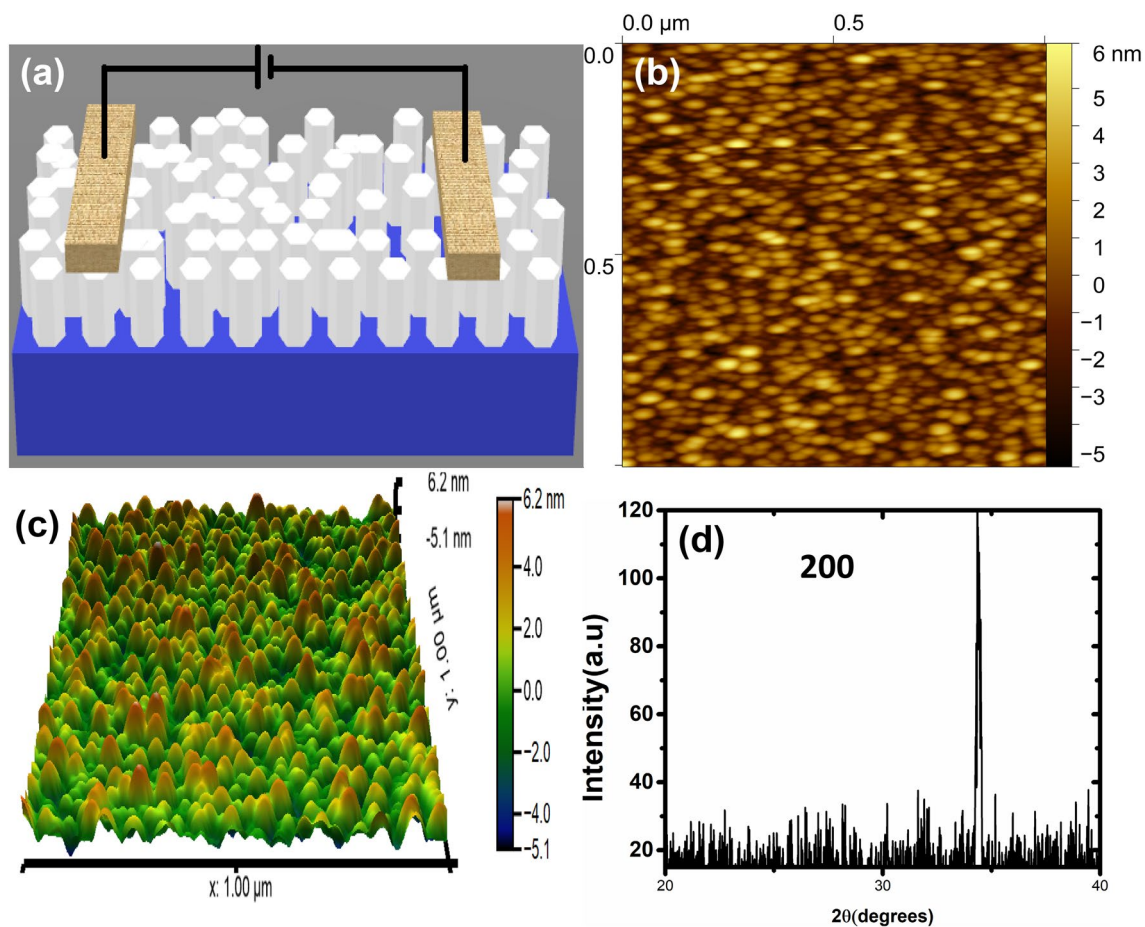


Fig. 1 **a** Schematic of the device, **b** two-dimensional AFM image of 80 nm ZnO seed layer, **c** three-dimensional AFM image of ZnO surface, **d** XRD spectra of 80 nm seed layer

film is estimated to be 5.5 nm using Gwyddion software for analysis of raw AFM data, and this indicates that the film surface was smooth. The ZnO thin film's XRD pattern is shown in Fig. 1d. The XRD data of the thin film showed only one reflection corresponding to the (002) plane of the wurtzite structure of ZnO, supporting the AFM result and indicating the highly *c*-axis-oriented thin film, where *c*-axis is considered to be normal to the substrate surface [7, 17].

The XRD patterns of ZnO nanorods in S1 and S2 are shown in Fig. 2a. A high-intensity peak at 34.4° of narrow FWHM, which represents the ZnO (002) plane, is observed in the phase pattern of the as-grown ZnO NRs in two precursors. The strong peak corresponding to (002) crystal plane indicates that the as-grown nanorods are of a single crystal phase of high quality and were grown parallel to the *c*-axis direction in samples S1 and S2 [7, 18].

An XPS measurement was performed to know the chemical features of nanorods in S1 and S2, and the results are shown in Fig. 2b. Peaks representing C1s, O1s, Zn 2p_{3/2}, and Zn 2p_{1/2} are identified from Fig. 2b and no other peaks were observed which indicate impurities of elements in

nanorods [7, 18]. The O1s peak obtained in survey spectra given in Fig. 2b of grown nanorods could be fitted to peaks located at 530.97 and 532.36 eV, with Gaussian fit. The two peaks located at 530.97 and 530.98 eV in survey spectra in ZnO nanorods could be attributed to the O²⁻ ions of ZnO crystalline phase [18].

Figure 2b shows that the peaks located at 1020.99 eV and 1044.12 eV are attributed to Zn2p_{3/2} and 2p_{1/2} levels, respectively, and it confirms the presence of a ZnO phase in samples S1 and S2 [7, 19]. EDX analysis of ZnO nanorods of samples S1 and S2 also indicate the high purity of the film. Figure 3a–d shows the top view and tilted SEM images of vertically oriented ZnO nanorods grown by the hydrothermal method over ZnO seeded substrates in two precursor solutions. Figure 3a, d low-magnification top view images show the uniformity of the nanostructure and a dislocation at the center of nanorods grown in zinc acetate precursor.

According to literature to engineer the nanostructure morphology of hydrothermally synthesized ZnO nanorods many growth parameters have been explored, including the seed layer thickness variation, addition of extra agents such as

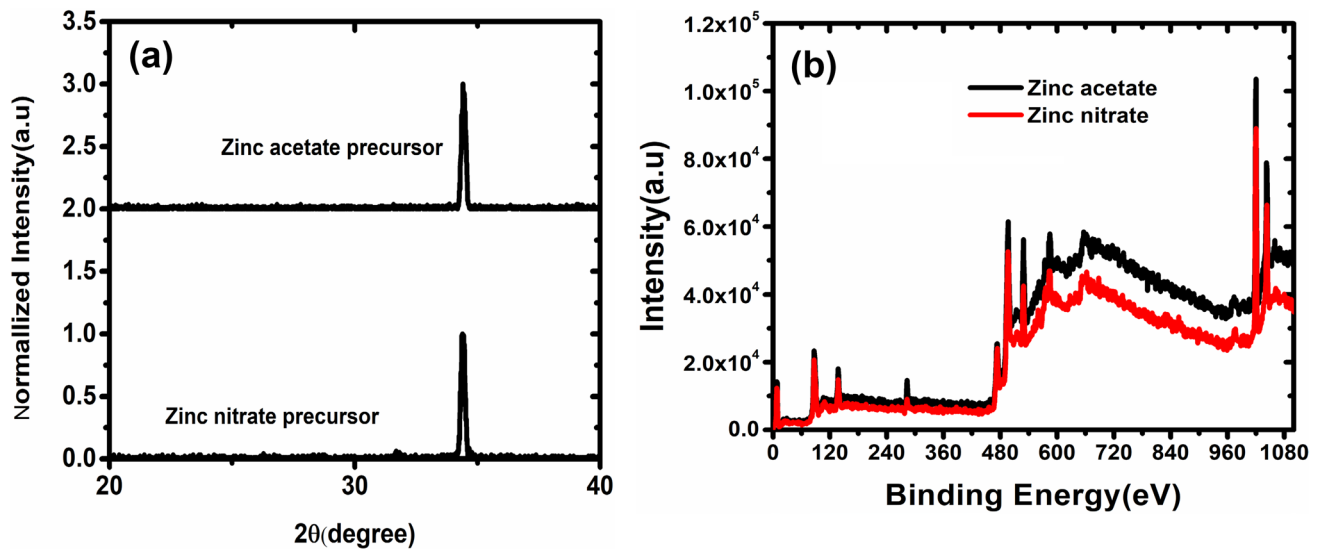


Fig. 2 **a** XRD spectra of nanorods grown by two precursors, **b** XPS spectra of nanorods grown by two precursors

organic ligands and some metal ions like cadmium, aluminum etc., here dislocation created owing to precursor chemistry [20]. Dislocation in NRs grown in zinc acetate precursor solution could be created via propagation of an axial screw dislocation during growth [21]. The pointed dislocation observed in NRs was grown in the zinc acetate precursor over 150–200 nm seeded substrate [7]. The dislocation in the present study was uniform and hexagonal throughout the sample compared to our previous study and could lead to better sensitivity compared to the conventional nanorods [7].

Figure 4a, b shows the current variation of the as-fabricated sensors over NRs grow in two precursors when exposed to a range of H_2 concentration from 4 to 24 ppm in the air at 27 °C. The current between the electrodes in all devices increased immediately after being exposed to a H_2 atmosphere. As obtained in Fig. 4a, b, the current variation of the sensor is larger, which is fabricated over NRs with dislocation than that of sensor which builds on the conventional nanorods and semilogarithmic plot of the devices is shown in Fig. 4c, d. This better performance of zinc acetate-synthesized NRs could be attributed to the improvement of the surface to volume ratio of dislocated NRs. The sensitivity defined in the terms of current instead of resistance of the two devices containing NRs which were grown in a different precursor solution is shown in Fig. 5a, b.

The sensitivity considering the current of the devices to the hydrogen is defined in Eq. (1) [1].

$$S = \frac{I_g - I_a}{I_a} \times 100. \quad (1)$$

Instead of the resistance, current is used in the present case to identify the correct value of the response for

real-time applications, although we have calculated series resistance to explain the sensing mechanism. The resistance which was assumed in most cases to define sensitivity could be varied with the voltage and contact resistance will also added when resistance was calculated by voltage and current ratio (Ohms law) [22–24]. The device sensitivity calculated as per Eq. (1) is plotted against different hydrogen concentrations as shown in Fig. 5a, b. The sensitivity in our case did not vary with the applied voltage largely, but its maximum value was at 0.7 V as exhibited in Fig. 5a, b. The important thing that could be noted is the resistance which we estimated here is responsible for the hydrogen sensing called as series resistance. While using the sensor in the field, the current is measured continuously which depends on resistance, so in our opinion measurement of the current flowing in devices as the function of gas concentration during the experiment could be more helpful in judging the quality of the sensor. In this type of measurement, operating voltage can easily be identified, so there is no need to measure resistance for each and every voltage for deciding the best operating point.

From Fig. 5a, b, it is seen that maximum sensitivity was achieved at 0.7 eV biasing voltage. The power consumed at this biasing voltage is 1.4×10^{-5} W and 3.5×10^{-6} W for sensor fabricated on NRs with dislocation and conventional NRs, respectively. The sensors developed in this study would be cost effective, detects gases at room temperature, avoids explosion and saves power. From Fig. 5a, b, it is evident that maximum sensitivity of sensor fabricated on NRs with dislocation is nearly six times than that of the sensor on the conventional NRs. This difference is because of the large surface area in dislocated nanorods, which could provide a significant reaction platform for hydrogen and adsorbed

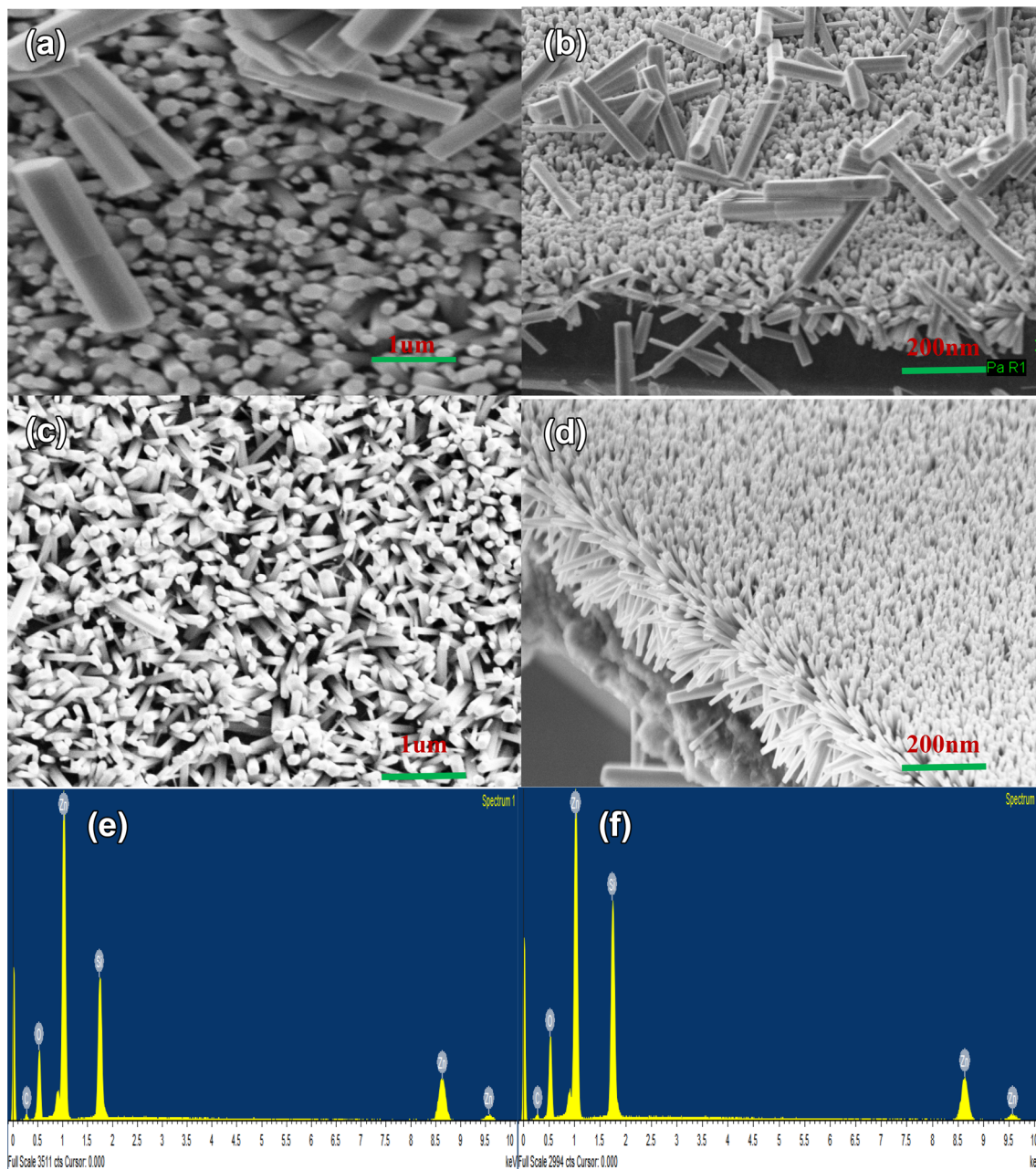


Fig. 3 **a** Top view scanning electron microscopy image of sample S1. **b** A tilted view of ZnO NRs on S1. **c** Top view scanning electron microscopy image of S2. **d** A tilted view of ZnO NRs on S2. **e** EDX spectra of sample S1. **f** EDX spectra of sample S2

oxygen. The time of response is defined as the time for the sensitivity to increase to 90% of its saturation value after the injection of gas to the chamber [1, 22, 23]. Similarly, the time of the recovery is defined as the time for the sensitivity to decrease to 90% of saturation value after H_2 is removed from the chamber [1, 22, 23]. The response time is 20 s and 19 s for devices fabricated over NRs with dislocation and conventional NRs, respectively. Recovery time is 30 s and 29 s for sensor fabricated on dislocated NRs and over the conventional NRs. The change in current considered here

for sensitivity measurement on hydrogen exposure is related to the series resistance. Series resistance is related to the intergrain potential [1]. Here we are trying to explain how device current changed in exposed hydrogen and quantify the quantity responsible for this. We have observed in our previous work the negative barrier height at the interface of Ti/Al and ZnO [23]. Thus, it can be guessed that barrier potential at the boundaries of grains could be the origin of the barrier potential at the interface of metal–semiconductor. So, the metal–semiconductor interface barrier could be

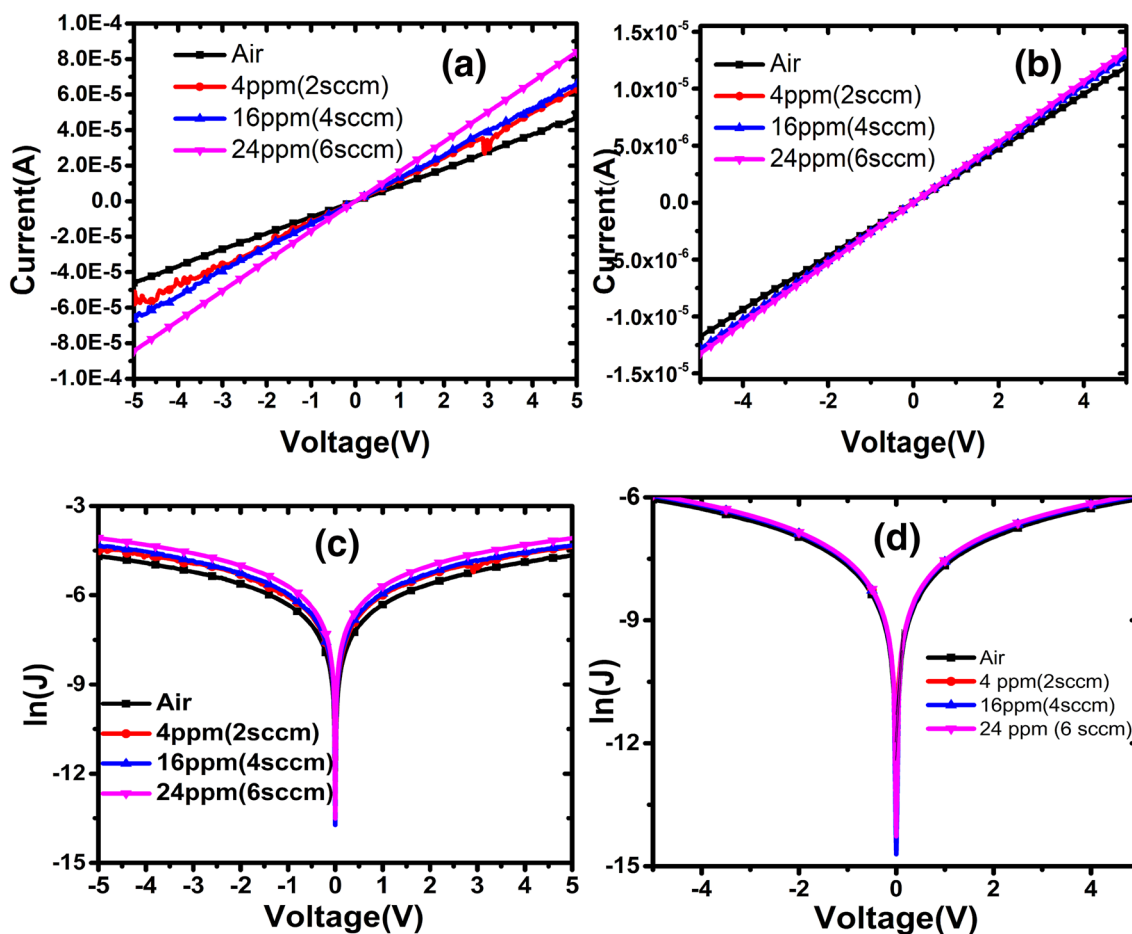


Fig. 4 *I*–*V* characteristics of the device in air and hydrogen atmosphere **a** device built on dislocated NRs **b** device built on conventional NRs **c** semilogarithmic plot device built on dislocated nanorods **d** semilogarithmic plot device built on conventional nanorods

a representative of the intergrain potential. Further, interface barrier potential of metal–semiconductor can be analyzed by fitting the *I*–*V* characteristics shown in Fig 5a, b with Eq. (2) and estimating the saturation current which is intercept in the semilogarithmic plot shown in Fig. 5c, d and placing saturation current value in Eq. (3) [22, 23].

$$I = I_0 \left(\exp \frac{q(V - IR_s)}{\eta KT} - 1 \right), \tag{2}$$

where “*I*” is current across the interface, “*I*₀” is reverse saturation current, “*η*” is ideality factor, “*T*” is operating temperature, “*R*_s” is the series resistance.

$$I_0 = A^* AT^2 \exp \frac{-q_s \Phi_b}{KT}, \tag{3}$$

where “*A**” is the Richardson constant, “*A*” is the area of the contact, “*Φ*_b” is the potential barrier at the interface of the metal and semiconductor, while the rest of the symbols were defined for the Eq. (2) [23, 24]. The variations of the

experimentally estimated barrier height, which are representative of the potential barrier between boundaries of the two neighboring grains, are shown in Fig 5c, d. The series resistance *R*_s which affects the barrier at the junction also related to the grain boundaries can be estimated by Eq. (4) [23, 24].

$$\frac{\partial V}{\partial \ln I} = \frac{\eta KT}{q} + IR_s, \tag{4}$$

Equation (4) is obtained by rearranging Eq. (2).

Series resistance *R*_s experimentally observed by plotting equation 4 using current voltage data shown in Fig 4a, b as the slope of this plot. The series resistance variation with concentration for dislocated NRs and conventional nanorods are shown in Fig. 5c, d.

The values of the barrier height and series resistance in different concentrations of hydrogen for conventional and dislocated NRs are given in the Table 1. Data presented in Table 1 and trends in Fig. 5c, d revealed that barrier height and series resistance decreases with increasing hydrogen concentration

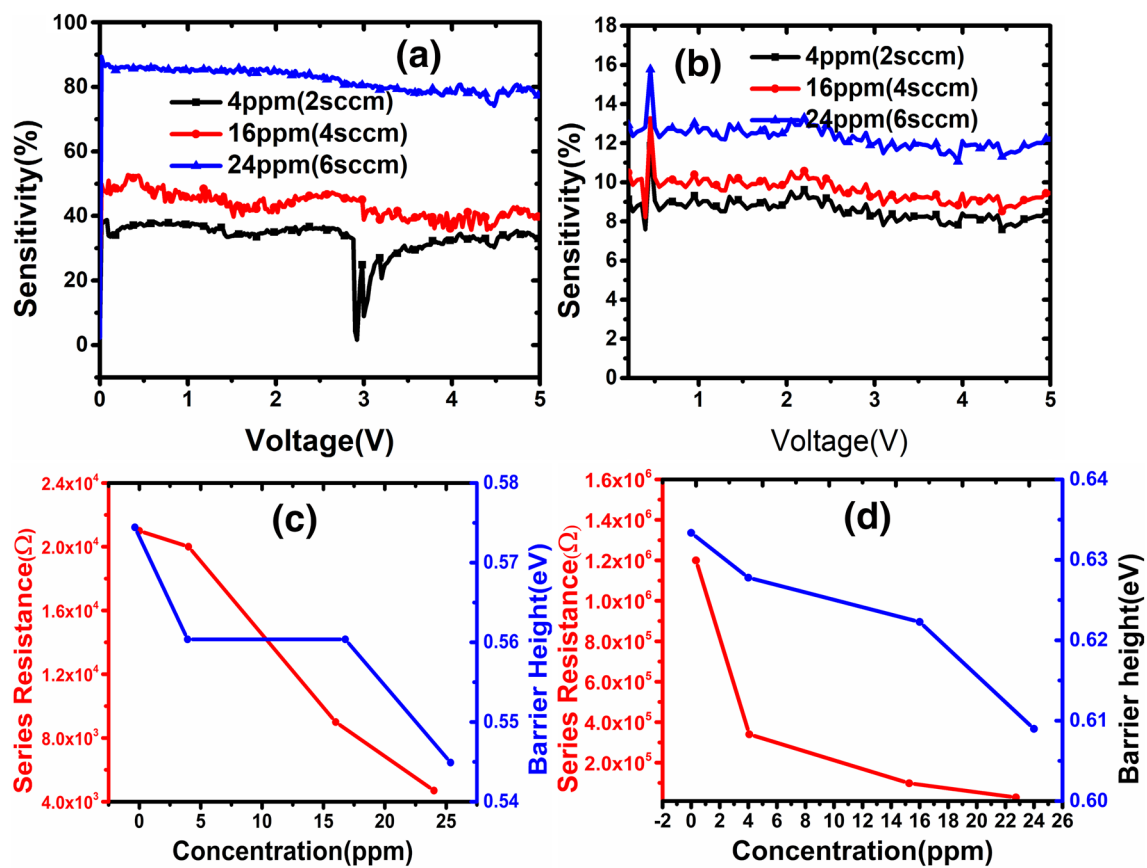


Fig. 5 Response of characteristics of the device in air and hydrogen atmosphere **a** device built on dislocated NRs **b** device built on conventional NRs **c** variation of series resistance and barrier height with

hydrogen gas concentration for dislocated NRs **d** variation of series resistance and barrier height with hydrogen gas concentration for conventional NRs

Table 1 Sensing results in different concentrations of the gas

Sensor	Concentration	Barrier height	Sensitivity (%)	Series resistance	Response/recovery
S11	0 ppm	0.574 eV	–	$2.1 \times 10^4 \Omega$	20 s/30 s
	4 ppm	0.560 eV	37.4%	$2.0 \times 10^4 \Omega$	
	16 ppm	0.558 eV	51.5%	$9 \times 10^3 \Omega$	
	24 ppm	0.544 eV	98%	$4.7 \times 10^3 \Omega$	
S22	0 ppm	0.633 eV	–	$1.2 \times 10^6 \Omega$	19 s/29 s
	4 ppm	0.627 eV	11.2%	$3.4 \times 10^5 \Omega$	
	16 ppm	0.622 eV	12.9%	$9.8 \times 10^4 \Omega$	
	24 ppm	0.608 eV	15.9%	$2.8 \times 10^4 \Omega$	

for both devices, which were grown in zinc acetate and zinc nitrate precursors. For the same concentration junction, barrier height representing the intergrain barrier for the nanorods grown in zinc acetate varied largely compared to zinc nitrate. A similar trend observed for the series resistance also. The barrier height slope was not uniform for the device built over ZnO nanorods grown in the zinc acetate but variation was large. The barrier height variation for the device built over the zinc nitrate-grown nanorods is uniform, but variation is not large. Series resistance of the device built over the zinc

acetate nanorods varies uniformly compared to that of device fabricated on the zinc nitrate nanorods. Series resistance of the device built over the zinc nitrate-grown nanorods show the saturation at a higher concentration. The series resistance depends on the conductivity of the ZnO and intergrain barrier potential, the relation between conductivity and intergrain potential is given in Eq. (5) [1].

$$\sigma = \sigma_0 \exp\left(\frac{-eV_s}{kT}\right) \quad (5)$$

where σ_0 is bulk intragranular conductance, k is the Boltzmann's constant, T is the absolute temperature, and eV_s is the inter grain potential barrier. The intergrain potential barrier is given by Eq. (6) [1]

$$eV_s = \frac{e^2 N_t^2}{2\epsilon_r \epsilon_0 N_d}, \quad (6)$$

where N_t is the surface density of adsorbed oxygen ions, $\epsilon_r \epsilon_0$ is permittivity of ZnO, and N_d is the concentration of electron donors. The change in intergrain barrier potential can be identified using series resistance, series resistance can obtain from conductivity and it is given in Eq. (7)

$$R_s = \frac{1}{\sigma} \frac{l}{A} = \frac{l}{A\sigma_0} \exp\left(\frac{eV_s}{kT}\right). \quad (7)$$

The series resistance being changed when hydrogen gas exposed to the device, it will be explained later in this article and in Eq. (6).

If we consider series resistance R_{so} in air and R_{sg} in gas, the corresponding intergrain potentials are eV_{so} and eV_{sg} and they related as per Eqs. 8 and 9, respectively.

$$R_{so} = \frac{1}{\sigma} \frac{l}{A} = \frac{l}{A\sigma_0} \exp\left(\frac{eV_{so}}{kT}\right), \quad (8)$$

$$R_{sg} = \frac{1}{\sigma} \frac{l}{A} = \frac{l}{A\sigma_0} \exp\left(\frac{eV_{sg}}{kT}\right). \quad (9)$$

On dividing Eq. (8) by Eq. (9), we get the change in the intergrain barrier, and this change is given in Eq. (10)

$$eV_{so} - eV_{sg} = e\Delta V = kT \ln\left(\frac{R_{so}}{R_{sg}}\right). \quad (10)$$

The change in the intergrain barrier obtained from the series resistance is three times that of change observed by the metal–semiconductor interface barrier. This close agreement provides an alternate method to identify the intergrain potential change just by measuring the change at the junction potential. This observation also proves formation of negative barrier height at the metal–semiconductor interface, which was identified by us in our previous work [22]. The intergrain barrier estimated is in close agreement with its previously observed values [25]. Adsorption and desorption of atmospheric oxygen on ZnO surface manipulating the intergrain potential as per Eq. (6) on NRs decides hydrogen sensing [26–29]. When a ZnO nanorod comes into contact with atmospheric oxygen and gases, their sensitivity towards other gases changes and depends upon the amount of adsorbed oxygen (O^- , O_2^- , and O_2^-) ions and defects if any, here nanorods with dislocation have been shown to have

better sensitivity [26]. At the beginning, when ZnO NRs come into contact with air, atmospheric oxygen is adsorbed on their surface and extracts the electron from the NRs and a depletion region is formed between the grains as given by Eq. (6). The magnitude of the depletion region and potential barrier are directly proportional to the square of the adsorbed oxygen and is governed by Eq. (6). Formation of this depletion region increases the resistance of NRs and decreases the total current conduction between the electrodes of the device fabricated over them [26–29]. When hydrogen gas is exposed to NRs, negative oxygen ion from the NRs immediately reacts with H_2 and forms water as product and as result of this reaction, electron is released on the surface of the NRs and reduces the barrier at the junction and increases the conductivity. As the conductivity increases, the series resistance is decreased and hence this increases the current conduction.

4 Conclusion

In summary, we have deposited 80 nm ZnO thin films as seed layer using RF sputtering technique. The particles in the seed layer are vertically oriented as observed from the AFM analysis and single crystalline as revealed from the XRD analysis. We employed two precursors zinc acetate and zinc nitrate to grow ZnO nanorods. A nanostructure dislocation was identified in nanorods grown in the zinc precursor solution. This dislocation provides better hydrogen sensitivity than the conventional NRs. The sensitivity showed by such nanorods is found to be maximum reported on conventional bare nanorods. We provide a platform to achieve better sensitivity at room temperature following conventional hydrothermal synthesis of ZnO nanorods by changing the precursors only. We were proposed a method probably for the first time to estimate the change in intergrain barrier height using simple I – V characteristics. We also proposed how series resistance which can be obtained from the current–voltage characteristic can be used to estimate the intergrain potential change.

Acknowledgements The authors' hearty thanks to Indian Nanoelectronics Users Program (INUP) at IIT Bombay for project number P1217182725 and Sophisticated Analytical Instruments Facility at IIT Bombay for completion of this work.

References

1. A.B. Yadav, S. Jit, Particle size effects on the hydrogen sensing properties of Pd/ZnO Schottky contacts fabricated by sol–gel method. *Int. J. Hydrog. Energy* **42**(1), 786–794 (2017)
2. S.Y. Chiu, H.W. Huang, K.C. Liang, K.-P. Liua, J.-H. Tsaib, W.S. Loura, Comprehensive investigation on planar type of Pd–GaN hydrogen sensors. *Int J Hydrog Energy* **34**(13), 5604–5615 (2009)

3. S. Basu, A. Dutta, Modified heterojunction based on zinc oxide thin film for hydrogen gas-sensor application. *Sens Actuator B* **22**(8), 3–7 (1994)
4. K.L.P. Thi, L.T. Nguyen, N.H. Ke, D.A. Tuan, T.Q.A. Le, L.V.T. Hung, The morphology and optical properties of ZnO nanorods grown on MoS₂ thin films at various thicknesses using a chemical bath deposition method. *J Electron Mater* **47**, 6302 (2018)
5. Dong-Hau Kuo, Jheng-Yu. He, Ying-Sheng Huang, Synthesis of vertically aligned ZnO nanorods on Ni-based buffer layers using a thermal evaporation process. *J Electron Mater* **41**, 451 (2012)
6. B.S. Sannakashappanavar, C.R. ByrareddyPesala, S. Kumar, A.B. Yadav, Superlattices Microstruct. **117**, 503–514 (2018)
7. K.H. Tam, C.K. Cheung, Y.H. Leung, A.B. Djuricic, C.C. Ling, C.D. Beling, S. Fung, W.M. Kwok, W.K. Chan, D.L. Phillips, L. Ding, W.K. Ge, Defects in ZnO nanorods prepared by a hydrothermal method. *J. Phys. Chem. B* **110**, 20865–20871 (2006)
8. J.X. Wang, X.W. Sun, H. Huang, Y.C. Lee, O.K. Tan, M.B. Yu, G.Q. Lo, D.L. Kwong, A two-step hydrothermally grown ZnO microtube array for CO gas sensing. *Appl. Phys. A* **88**, 611 (2007). <https://doi.org/10.1007/s00339-007-4076-8>
9. A. Zainelabdin, S. Zaman, G. Amin, O. Nur, M. Willander, Optical and current transport properties of CuO/ZnO nanocoral p–n heterostructure hydrothermally synthesized at low temperature. *Appl. Phys. A* **108**, 921 (2012). <https://doi.org/10.1007/s00339-012-6995-2>
10. Shu-Yi Liu, Tao Chen, Jing Wan, Ru Guo-Ping, Bing-Zong Li, Qu Xin-Ping, The effect of pre-annealing of sputtered ZnO seed layers on growth of ZnO nanorods through a hydrothermal method. *Appl. Phys. A* **94**, 775 (2009). <https://doi.org/10.1007/s00339-008-4957-5>
11. L.C. Tien, P.W. Sadik, D.P. Norton, L.F. Voss, S.J. Pearton, Hydrogen sensing at room temperature with Pt-coated ZnO thin films and nanorods. *Appl. Phys. Lett.* **87**, 222106 (2005)
12. H.T. Wang, B.S. Kang, F. Ren, L.C. Tien, P.W. Sadik, D.P. Norton, S.J. Pearton, J. Lin, Hydrogen-selective sensing at room temperature with ZnO nanorods. *Appl. Phys. Lett.* **86**, 243503 (2005)
13. Sapana Ranwa, Mohit Kumar, Jitendra Singh, Mattia Fanetti, Mahesh Kumar, Schottky-contacted vertically self-aligned ZnO nanorods for hydrogen gas nanosensor applications. *J. Appl. Phys.* **118**, 034509 (2015)
14. V.S. Bhati, S. Ranwa, M. Fanetti, M. Valant, M. Kumar, Efficient hydrogen sensor based on Ni-doped ZnO nanostructures by RF sputtering. *Sens. Actuators B* **255**, 588–597 (2018)
15. H. Kim, Y. Pak, Y. Jeong, W. Kim, J. Kim, G.Y. Jung, Amorphous Pd assisted H₂ detection of ZnO nanorod gas sensor with enhanced sensitivity and stability. *Sens. Actuators B Chem.* **262**(1), 460–468 (2018)
16. Hu Xiulan, Yoshitake Masuda, Tatsuki Ohji, Kazumi Kato, Micropatterning of ZnO nanoarrays by forced hydrolysis of anhydrous zinc acetate. *Langmuir*. **24**, 7614–7617 (2008)
17. Shibu Saha, Vinay Gupta, Influence of surface defects in ZnO thin films on its biosensing response characteristic. *J. Appl. Phys.* **110**, 064904 (2011)
18. Shu-Yi Liu, Tao Chen, Yu-Long Jiang, Ru Guo-Ping, Qu Xin-Ping, The effect of postannealing on the electrical properties of well-aligned nZnO nanorods/p-Si heterojunction. *J. Appl. Phys.* **105**, 114504 (2009)
19. M. Wang, F. Ren, G. Cai, Y. Liu, S. Shen, L. Guo, Activating ZnO nanorod photoanodes in visible light by Cu ion implantation. *Nano Res.* **7**, 353–364 (2014)
20. J. Joo, B.Y. Chow, M. Prakash, E.S. Boyden, J.M. Jacobson, Face-selective electrostatic control of hydrothermal zinc oxide nanowire synthesis. *Nat. Mater.* **10**, 596–601 (2011)
21. S.A. Morin, M.J. Bierman, J. Tong, S. Jin, Mechanism and kinetics of spontaneous nanotube growth driven by screw dislocations. *Science* **328**, 476–480 (2010)
22. R. Jaggi, Deviations from Ohm's law in semiconductors. *Phys. Chem. Solids* **29**, 1699–1702 (1968)
23. A.B. Yadav, S.S. Basavaraj, True Ohmic contact on RF sputtered ZnO thin film by using the nonalloy Ti/Au metallization scheme. *J Alloys Compd* **770**, 701–709 (2019). <https://doi.org/10.1016/j.jallcom.2018.08.166>
24. J.H. Werner, Schottky barrier and pn-junction I/V plots-small signal evaluation. *Appl. Phys. A* **47**, 291–300 (1988)
25. J. Ouerfelli, M. Regragui, M. Morsli, G. Djeteli, K. Jondo, C. Amory, G. Tchangbedji, K. Napo, J.C. Bernede, Properties of ZnO thin films deposited by chemical bath deposition and post annealed. *J. Phys. D Appl. Phys.* **39**, 1954–1959 (2006)
26. O. Ovsianyskyi, Y.S. Nam, O. Tsymbalenko, P.T. Lan, M.W. Moon, K.B. Lee, Highly sensitive chemiresistive H₂S gas sensor based on graphene decorated with Ag nanoparticles and charged impurities. *Sens. Actuators B Chem.* **257**, 278–285 (2018)
27. M.R. Modaberi, R. Rooydell, S. Brahma, A.A. Akande, B.W. Mwakikunga, C.P. Liu, Enhanced response and selectivity of H₂S sensing through controlled Ni doping into ZnO nanorods by using single metal organic precursors. *Sens. Actuators B Chem.* **273**, 1278–1290 (2018)
28. S. Ranwa, P.K. Kulriya, V.K. Sahu, L.M. Kukreja, M. Kumar, Defect-free ZnO nanorods for low temperature hydrogen sensor applications. *Appl. Phys. Lett.* **105**, 213103 (2014)
29. K. Yadav, S.K. Gahlaut, B.R. Mehta, J.P. Singh, Photoluminescence based H₂ and O₂ gas sensing by ZnO nanowires. *Appl. Phys. Lett.* **108**, 071602 (2016)

Publisher's Note Springer Nature remains neutral with regard to jurisdictional claims in published maps and institutional affiliations.